Preprints of the 21st IFAC World Congress (Virtual)
Berlin, Germany, July 12-17, 2020

Passivity-Based PI Control for AGVs Wireless Power Transfer System

Jia Liu * **Zhitao Liu** * **Hongye Su** *

* *State Key Laboratory of Industrial Control Technology, Institute of Cyber-Systems and Control, Zhejiang University, Hangzhou, China (e-mail: liujia1019@zju.edu.cn; ztliu@zju.edu.cn; hysu@iipc.zju.edu.cn)*

Abstract: Automatic guided vehicles (AGVs) recently have gained increasing attentions and applications, however, frequently stopping to recharge largely reduces service efficiency. Wireless power transfer (WPT) is considered as a practice energization way to solve this problem. In this paper, a passivity-based controller (PBC) and parameter designing method for compensation topology are proposed for AGVs WPT system. The PBC based on port-controlled Hamiltonian system (PCHS) is designed to achieve desired constant systematic working power by regulating the output voltage of DC/DC converter. The LCC-LCC resonant network is analyzed in the principle of the impedance matching method, and a proportional integral (PI) controller is implemented to realize zero steady-state error. Simulation are carried out in PLECS to verify analysis, and results show that proposed controller scheme and compensation designing method ensure the stability of the charging system against load variations, and the fast response performance of the control algorithm is also validated.

Keywords: Automatic guided vehicles (AGVs), wireless power transfer (WPT), impedance matching method, DC/DC converter, passivity-based control (PBC).

1. INTRODUCTION

Automatic guided vehicles (AGVs), also referred to as mobile robot with guidance device and motor control system, have been rapidly development in logistics industry Lu (2019). Stopping for charging reduces a lot of effective working time, resulting in low utilization rate and high use cost. With flexible charging position, safety and good adaptability, wireless power transfer (WPT) has drawn the attention of researchers RamRakhyani (2010); Zhang (2018) and it is meaningful to apply wireless charging to AGVs Lu (2019).

The compensation network is composed of loosely coupled transformer and external passive inductors or capacitors, which is the most important part in the design of a wireless charging system. According to the different series and parallel combination, there are four basic resonant compensation networks, i.e., series-series (SS), series-parallel (SP), parallel-series (PS) and parallel-parallel (PP) Zhang (2018); Feng (2016). In order to achieve a higher design degree, more higher order compensation network with more compensation elements is introduced. With current source characteristic and high efficiency, the LCC-LCC resonant compensation network is the most popular compensation topology Feng (2016); Li (2014). In addition, with the changing state of charge (SOC), the internal resistor

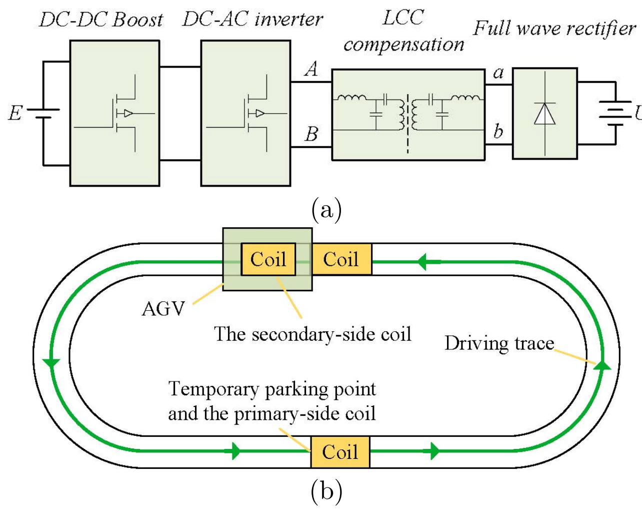

Fig. 1. The WPT system for AGVs. (a) The structure of this system. (b) An universal application scenario.

characteristics of onboard battery changes dynamically. In order to obtain a stable operation, the resonant state must be independent of the load conditions Xiao (2018). In this paper, the impedance matching method is introduced to design the network parameters and the transfer power of this network has been analysed.

Fig. 1(a) shows the structure of WPT system for AGVs, which consists of the primary side and the secondary side. Fig. 1(b) describes an universal application scenario. As the energy transmitter, certain primary sides are preplaced at this stops on the driving trace. The secondary

⋆ This work was partially supported by National Key R&D Program of China (Grant NO. 2018YFA0703800); Science Fund for Creative Research Group of the National Natural Science Foundation of China (Grant NO.61621002), National Natural Science Foundation of China (NSFC:61873233, 61633019), Fundamental Research Funds for the Central Universities.

side is installed on the AGV chassis to pick up energy Lu (2019). It starts to work when the AGV arrives and stops at this parking points to handle the preset task, then energy can be transferred from primary side to secondary side during the parking gap. When the task is completed, AGV arrives to the next stop. With the intermittent charging during the parking gap, the 24-hour intelligent working mode is achieved, which not only increases efficient working time with a high utilization rate, but also reduces onboard battery pack and initial cost Zhang (2018).

For the typical voltage of the onboard battery is 24 V, the charging current can reach 75 A with 1.8kW transfer power. In order to improve the transfer power, full wave rectifier with a high frequency transformer is connected with the LCC-LCC compensation network to increase the output voltage of this resonant network, which is proportional to the transfer power. A DC-DC Boost converter is added to regulate the transfer power by regulate the output voltage, i.e., the input voltage of this resonant network, resulting in a high nonlinear and unknown load to this converter.

The control method for this system is the another significant aspect. A lot of researches have been done for the controller of DC/DC Boost converter. In these control algorithms, passivity-based control (PBC) as a non-linear control method, has been widely applied in power electronics including DC/DC Boost converter. Several researchers have applied PBCs to control the output voltage of boost converter Jeltsema (2004); Ortega (2004). Without consideration of the parasitic parameters, these controller cannot maintain robust with load variations. Taking the parasitic resistor into consideration, a output feedback controller is proposed to achieve desired output voltage against load uncertainty Son (2011). However, since this controller is extremely complex, the algorithm is not easy to be implemented. Due to the high nonlinear and unknown load, it is not easy to design an algorithm that is robust against variable load Zeng (2014). Without consideration of the uncertain parasitic resistors, this paper proposes a easily implemented passivity-based proportional integral (PI) controller. In another word, a complementary PI controller is designed and combined with PBC to eliminate the steady-state error when the load changes, resulting in a easy implemented and strong robust controller.

The compensation topology and control algorithm are the most significant and tough to design in the field of WPT system. The contribution of this paper is to propose a parameter design method for compensation circuit based on impedance matching method, and a PBC scheme is also applied to wireless charging system. With the proposed parameter designing method and PBC, a stable resonance is achieved to ensure the stability of the AGVs wireless charging system. Moreover, a PI controller is presented to work with the PBC to eliminate the steady-state error against load variations.

This paper is organized as follows. In section 2, the analysis of the LCC-LCC compensation is studied, and the impedance matching method also can be obtained. The passivity-based PI controller is proposed in Section 3. The AGVs wireless charging system is presented in section 4, while some simulations are also carried out in PLECS. Finally, Section 5 presents the conclusions.

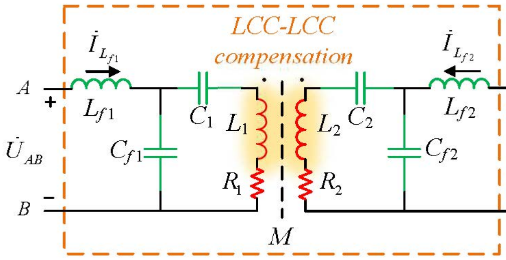

Fig. 2. The LCC-LCC compensation network

2. ANALYSIS ON THE LCC-LCC COMPENSATION NETWORK

2.1 LCC-LCC Compensation Network

As shown in Fig. 2, L_1 and L_2 are the primary coil and the secondary coil, and the alternating current (AC) equivalent resistors are R_1 and R_2, respectively. L_{f1} and C_{f1} are the primary resonant inductor and capacitor, respectively. L_{f2} and C_{f2} are the secondary resonant inductor and capacitor, respectively. C_1 and C_2 are the primary and the secondary compensation capacitors, respectively. M is the mutual inductor between the two coils.

2.2 Impedance Matching for Two-Port Network

Due to mutual coupling, the LCC-LCC compensation network can be described as a two-port network. Suppose that the input voltage between the port $A - B$ is $\dot{U}_{AB}$ and the output voltage between the port $a - b$ is $\dot{U}_{ab}$. The current flowing through the primary coil and the secondary coil are $\dot{I}_1$ and $\dot{I}_2$. $\dot{I}_{L_{f1}}$ and $\dot{I}_{L_{f2}}$ represent the currents on L_{f1} and L_{f2}. ω denotes the working angular frequency and the frequency is f. The two-port network can be expressed as

$$\begin{bmatrix} \dot{U}_{AB} \\ \dot{U}_{ab} \end{bmatrix} = \begin{bmatrix} Z_{11} & Z_{12} \\ Z_{21} & Z_{22} \end{bmatrix} \begin{bmatrix} \dot{I}_{Lf1} \\ \dot{I}_{Lf2} \end{bmatrix} \tag{1}$$

where

$$\begin{cases} Z_{11} = j\left[H_{11} - (H_{21} - jR_2)/\left(\omega^2 C_{f1}^2 H_3\right)\right] \\ Z_{21} = Z_{12} = j\omega M/(\omega^2 C_{f1} C_{f2} H_3) \\ Z_{22} = j\left[H_{22} - (H_{12} - jR_1)/\left(\omega^2 C_{f2}^2 H_3\right)\right] \end{cases}, \tag{2}$$

$$\begin{cases} H_{11} = \omega L_1 - (\omega C_1)^{-1} - (\omega C_{f1})^{-1} \\ H_{12} = \omega L_{f1} - (\omega C_{f1})^{-1} \\ H_{22} = \omega L_2 - (\omega C_2)^{-1} - (\omega C_{f2})^{-1} \\ H_{21} = \omega L_{f2} - (\omega C_{f2})^{-1} \\ H_3 = (H_{21} - jR_2)(H_{12} - jR_1) - \omega^2 M^2 \end{cases}. \tag{3}$$

The open-circuit and short-circuit method is introduced to solve the network parameters. When the $\dot{U}_{ab}$ is applied on port $a - b$, the open-circuit voltage (OCV) can be derived as $\dot{U}_{ABOC} = \dot{U}_{AB}\Big|_{\dot{I}_{Lf1}=0} = -\frac{Z_{12}}{Z_{22}}\dot{U}_{ab}$, and the short-circuit current (SCC) can be obtained as $\dot{I}_{Lf1SC} = \dot{I}_{Lf1}\big|_{\dot{U}_{AB}=0} = \frac{Z_{12}}{Z_{12}^2 - Z_{11}Z_{22}}\dot{U}_{ab}$. Then, the equivalent impedance Z_{eq1} between port $A-B$ can be expressed as follows

$$Z_{eq1} = \frac{\dot{U}_{ABOC}}{\dot{I}_{Lf1SC}} = \frac{Z_{11}Z_{22} - Z_{12}^2}{Z_{22}} \tag{4}$$

Similarly, when the $\dot{U}_{AB}$ is applied on port $A - B$, we can derive that OCV is $\dot{U}_{abOC} = \dot{U}_{ab}\Big|_{\dot{I}_{Lf2}=0} = \frac{Z_{12}}{Z_{11}}\dot{U}_{AB}$, and the short-circuit current (SCC) is $\dot{I}_{Lf2SC} = \dot{I}_{Lf2}\Big|_{\dot{U}_{ab}=0} = \frac{Z_{12}}{Z_{12}^2 - Z_{11}Z_{22}}\dot{U}_{AB}$. Then, we obtain the equivalent impedance Z_{eq2} between port $a - b$

$$Z_{eq2} = \frac{\dot{U}_{abOC}}{\dot{I}_{Lf2SC}} = \frac{Z_{12}^2 - Z_{11}Z_{22}}{Z_{11}} \tag{5}$$

Substituting (2) into (4) and (5), respectively. We obtain

$$\begin{aligned} Z_{eq1} &= \frac{\omega^2 M^2}{\omega^2 C_{f1}^2 H_3 \left[R_1 - j(\omega^2 C_{f2}^2 H_3 H_{22} - H_{12})\right]} \\ &\quad -j(H_{12} - \frac{H_{21}}{\omega^2 C_{f1}^2 H_3}) \end{aligned} \tag{6}$$

$$\begin{aligned} Z_{eq2} &= \frac{\omega^2 M^2}{\omega^2 C_{f2}^2 H_3 \left[R_2 - j(\omega^2 C_{f1}^2 H_3 H_{11} - H_{21})\right]} \\ &\quad -j(H_{21} - \frac{H_{12}}{\omega^2 C_{f2}^2 H_3}) \end{aligned} \tag{7}$$

When the two-port network operates in the resonant state, the input and output equivalent impedance of this network must be the smallest. Thus, the maximum transfer power and the maximum transfer efficient can be achieved. According to the resonance theorem, the imaginary part of the input and output impedances should be 0, i.e., $Im(Z_{eq1}) = Im(Z_{eq2}) = 0$. Then, from (6) and (7), we get

$$H_{11} = H_{12} = H_{22} = H_{21} = 0 \tag{8}$$

Combining (3) with (8) yiels the resonant condition

$$\begin{cases} \omega L_1 - (\omega C_1)^{-1} - (\omega C_{f1})^{-1} = 0 \\ \omega L_{f1} - (\omega C_{f1})^{-1} = 0 \\ \omega L_2 - (\omega C_2)^{-1} - (\omega C_{f2})^{-1} = 0 \\ \omega L_{f2} - (\omega C_{f2})^{-1} = 0 \end{cases} \tag{9}$$

With the impedance matching method, a stable resonance is easy to be achieved according to (9). The resonant conditions of primary-side and secondary-side are only related to their own circuit parameters, which are independent of mutual inductor and output load.

2.3 Transfer Power of the Network

While R_1 and R_2 are too small to influence the system, in order to facilitate the analysis and design, the AC equivalent resistors are regarded as 0, i.e., $R_1 = R_2 = 0$.

When the LCC-LCC network is working in the resonant state, the series connection of resonant inductor and resonant capacitor on each side can be regarded as a low-pass filter, resulting in the attenuation of high frequency components. Therefore, fundamental frequency components of the voltage and current on the two coils play a dominant role, which can be regarded as sinusoidal wave.

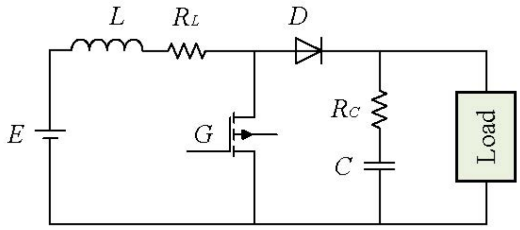

Fig. 3. The topology of DC/DC Boost converter

Assuming that $\dot{U}_{AB}$ and $\dot{U}_{ab}$ are the fundamental frequency components of the excitation source at the primary side and secondary side, respectively. $\dot{I}_{Lf1}$ and $\dot{I}_{Lf2}$ represent the fundamental frequency components of the currents on resonant inductors. In order to analyze the phase relation of current and voltage, assume $\dot{U}_{AB}$ is the reference value, i.e., $\dot{U}_{AB} = U_{AB}\angle 0°$, we get

$$\dot{U}_{ab} = \frac{\dot{U}_{AB}}{j} = U_{ab}\angle\varphi = U_{ab}\angle - 90° \tag{10}$$

where φ is the phase by which U_{ab} leads U_{AB}, U_{AB} and U_{ab} are the root mean square (RMS) of the fundamental components. Spelling out (1) and combining (10) yields

$$\begin{aligned} \dot{I}_{Lf1} &= -\frac{M\dot{U}_{ab}}{j\omega L_{f1}L_{f2}} = \frac{MU_{ab}}{\omega L_{f1}L_{f2}}\angle 0° \\ \dot{I}_{Lf2} &= \frac{M\dot{U}_{AB}}{j\omega L_{f1}L_{f2}} = \frac{MU_{AB}}{\omega L_{f1}L_{f2}}\angle - 90° \end{aligned} \tag{11}$$

From (11), we can get that the voltage and current on both sides of the network are in phase, thus, the unit power factor is achieved. What's more, the phase relation between voltage and current is independent of the coupling condition and load condition. The transfer power can be expressed by

$$P = \dot{U}_{AB} \cdot \dot{I}_{Lf1} = \frac{M}{\omega L_{f1}L_{f2}}U_{AB}U_{ab} \tag{12}$$

It is clear that this transfer power is proportional to the mutual inductor M, primary voltage U_{AB}, and secondary voltage U_{ab}. Therefore, a DC/DC Boost converter is added before this network to control the transfer power by regulating the primary voltage.

3. PASSIVITY-BASED PI CONTROL

3.1 Modelling a DC/DC Boost Converter

Fig. 3 shows the topology of the DC/DC Boost converter. The parasitic resistors in inductor and capacitor are R_L and R_C, respectively. Due to the complexity of the rear circuit, the load of this Boost converter, which consists of resonant network, full ware rectifier and the onboard battery, is of high nonlinear. For simplicity, the load of this converter is expressed as load and denoted by R. Assuming that the converter works in the continuous current mode (CCM) and $R_L = R_C = 0$, then, the average model is given by

$$\begin{cases} \dfrac{di}{dt} = \dfrac{E}{L} - \dfrac{(1-d)}{L}v \\ \dfrac{dv}{dt} = -\dfrac{v}{CR} + \dfrac{(1-d)}{C}i \end{cases} \tag{13}$$

where i and v represent, respectively, the input inductor current and the output voltage on capacitor; E is the external input voltage; and d represents the duty ratio of IGBT.

3.2 Passivity-Based Control

The dynamic system (13) can be written as a port-controlled hamiltonian (PCH) form as follows:

$$\begin{cases} \dot{x} = [J(x) - R(x)] \cdot \dfrac{\partial H(x)}{\partial x} + \zeta + g(x)u \\ y = g^{\mathrm{T}}(x)\dfrac{\partial H(x)}{\partial x} \end{cases} \tag{14}$$

where $x \in R^n$ is the state vector; J, R: $R^n \to R^{n\times n}$ are the interconnection and dissipation matrices, respectively, with $J(x) = -J^{\mathrm{T}}(x)$ and $R(x) = R^{\mathrm{T}}(x)$; H: $R^n \to R$ is the total stored energy function; g: $R^n \to R^{n\times m}$ is the input matrices; ζ represents the external force; and u, $y \in R^m$, $m < n$, are the control action and the output function, respectively.

From the energy view point, the storage energy function of the dynamic system can be expressed as

$$H(x) = \frac{1}{2}x^{\mathrm{T}}Qx \tag{15}$$

where $x = (x_1, x_2)^{\mathrm{T}} = (L \cdot i, C \cdot v)^{\mathrm{T}}$, x_1 and x_2 represent the inductance flux and the charge in the capacitance, $Q \in R^{n\times n}$ is a diagonal symmetric matrix representing the circuit parameters and $Q = diag\{1/L, 1/C\}$. Combing (13) with (14) we get

$$J(x) = \begin{pmatrix} 0 & -1 \\ 1 & 0 \end{pmatrix}, R(x) = \begin{pmatrix} 0 & 0 \\ 0 & 1/R \end{pmatrix},$$
$$\zeta = (E, 0)^{\mathrm{T}}, g(x) = \begin{pmatrix} x_2/C \\ -x_1/L \end{pmatrix}.$$

In this paper, the expected energy function of system (14) can be written as (16), let x^* is an admissible equilibrium point of x, and $\tilde{x} := x - x^*$.

$$H_d(x) = \frac{1}{2}\tilde{x}^{\mathrm{T}}Q\tilde{x} \tag{16}$$

Assume there are matrices $J_d(x) = -J_d^{\mathrm{T}}(x)$, $R_d(x) = R_d^{\mathrm{T}}(x) \geq 0$ and $H_d(x)$ is such that

$$x^* = \arg\min H_d(x) \tag{17}$$

Then, assume there exists $u = \beta(x)$, the closed-loop dynamic system (14) can be rewritten as follows

$$\dot{x} = [J_d(x) - R_d(x)]\frac{\partial H_d(x)}{\partial x} \tag{18}$$

with x^* a stable equilibrium. According to La Salle's invariant principle, if the largest invariant set under the closed-loop dynamics (18) contained in

$$\left\{x \in R^n | \frac{\partial H_d^{\mathrm{T}}(x)}{\partial x} R_d \frac{\partial H_d(x)}{\partial x} = 0\right\} \tag{19}$$

equals $\{x^*\}$. Then, the closed-loop system is asymptotically stable.

Proof. Substituting $u = \beta(x)$ into (14) yields (18). Since $J_d(x)$ is negative-symmetric Matrix and $R_d(x)$ is positive-symmetric Matrix, the time derivative of the storage function is obtained

$$\dot{H}_d(x) = -\left(\frac{\partial H_d(x)}{\partial x}\right)^{\mathrm{T}} R_d \frac{\partial H_d(x)}{\partial x} \leq 0 \tag{20}$$

then, x^* is a stable equilibrium point and $H_d(x)$ can be regarded as a Lyapunov function. Based on La Salle's invariant principle and the conclusion (19), the dynamic system is proved to be asymptotically stable.

Combining (14) with (18), we have

$$\begin{aligned} &[J_d(x) - R_d(x)]\frac{\partial H_d(x)}{\partial x} \\ &= [J(x) - R(x)]\frac{\partial H(x)}{\partial x} + \zeta + g(x)u \end{aligned} \tag{21}$$

Assuming that $H_d(x) = H(x) + H_a(x)$, $J_d(x) = J(x) + J_a(x)$, $R_d(x) = R(x)+R_a(x)$, $u = d$ is the duty ratio of the IGBT and $K(x) = \partial H_a(x)/\partial x = \partial H_d(x)/\partial x - \partial H(x)/\partial x$. Let $J_d(x) = 0$, $R_d(x) = diag(r_1, 1/r_2)$, where r_1 and r_2 are the injected virtual impedances. Then, (21) can be taken as follows

$$\begin{aligned} &[J_d(x) - R_d(x)]\frac{\partial H_a(x)}{\partial x} \\ &= -[J_a(x) - R_a(x)]\frac{\partial H(x)}{\partial x} + \zeta + g(x)u \end{aligned} \tag{22}$$

where

$$J_a(x) = \begin{pmatrix} 0 & 1 \\ -1 & 0 \end{pmatrix},$$
$$R_a(x) = \begin{pmatrix} r_1 & 0 \\ 0 & 1/r_2 - 1/R \end{pmatrix},$$
$$K(x) = (\, -x_1^*/L \;\; -x_2^*/C \,).$$

Now, (22) can be further simplified, that is

$$\begin{cases} \dfrac{x_1^*}{L}r_1 = \dfrac{r_1}{L}x_1 + \dfrac{d-1}{C}x_2 + E \\ \dfrac{x_2^*}{C}\dfrac{1}{r_2} = \dfrac{1-d}{L}x_1 + \dfrac{1}{r_2 C}x_2 - \dfrac{1}{RC}x_2 \end{cases} \tag{23}$$

Here, substituting x_1, x_2 into (23), we get

$$I^* r_1 = i \cdot r_1 + v(d-1) + E \tag{24}$$

$$\frac{V^*}{r_2} = i(1-d) + \frac{v}{r_2} - \frac{v}{R} \tag{25}$$

where V^* and I^* are the expected steady-state values of v and i, here, the duty ratio can be obtained

$$d = \frac{v - E + r_1(I^* - i)}{v} \tag{26}$$

Assuming that the loss in the DC/DC converter is neglected, the relationship between the steady-state value of output voltage and the steady-state value of inductance current can be obtained law of conservation of energy, when the system reaches a stable state, that is

$$I^* = \frac{V^{*2}}{ER} \tag{27}$$

Combining (27) with (28), the duty ratio becomes

$$d = \frac{v - E + r_1(V^{*2}/ER - i)}{v} \tag{28}$$

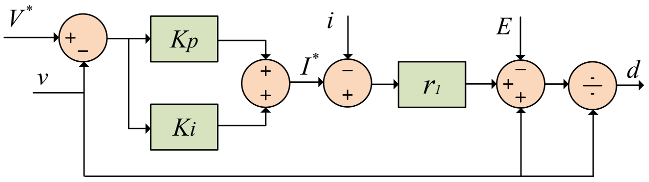

Fig. 4. The scheme of the controller

3.3 Complementary PI Controller

In order to simplify the modelling of DC/DC converter, the loss of IGBT, parasitic resistors of components and power loss caused by parasitic parameters have been neglected. Therefore, according to the law of energy conservation, the input power of the converter circuit equals its output power. However, the power loss mentioned above can not be neglected in practice. Due to the load variations and uncertainties of system parameters, the system can not be able to reach the desired output voltage without a steady-state error using (28). What's more, the load of the DC/DC converter, consists of several different and complex circuit modules, which cannot be just simplified as a resistor load R. Then, a PI controller is introduced and combined with the (26) to eliminate the steady-state error, resulting in a passivity-based PI controller. Fig. 4 shows the scheme of the controller for this system.

4. SIMULATION RESULTS

Simulations are carried out in PLECS to validate the proposed controller. Table 1 shows parameters of this system. The dynamical changed battery voltage with the SOC is simulated by the controlled voltage source. The control goal is to obtain desired charging power by regulating the output voltage of DC/DC converter with respect to the variable load condition. And a fair comparison test applied PID algorithm, which is referred as dual closed-loop PI control, is also implemented.

Table 1. system parameters

Parameter	Value	Unit
Primary resonant inductor L_{f1}	47.10	μH
Secondary resonant inductor L_{f2}	46.81	μH
primary resonant capacitor C_{f1}	74.44	nF
Secondary resonant capacitor C_{f2}	74.90	nF
Primary compensation capacitor C_1	97.93	nF
Secondary compensation capacitor C_2	101.74	nF
Primary coil L_1	82.90	μH
Secondary coil L_2	81.27	μH
Mutual inductor M	26.28	μH
Resonant frequency f	85	kHz
Battery voltage U_b	22 – 28	V
Switching frequency f_s	20	kHz
Capacitor of Boost C	400	μF
Inductor of Boost L	2500	μH
Parasitic resistor of R_C	10	$m\Omega$
Parasitic resistor of R_L	10	$m\Omega$
Nominal output voltage V^*	650	V
External input voltage E	310	V

In the simulation tests, this controlled voltage is step changed between $22V$ to $28V$, which is the disgusting load variation. According to the variable battery voltage, we can identify three distinct modes: mode 1: the battery voltage is unchanged at $22V$; mode 2: the voltage is step changed from $22V$ to $28V$; mode 3: the voltage is step changed from $28V$ back to $22V$.

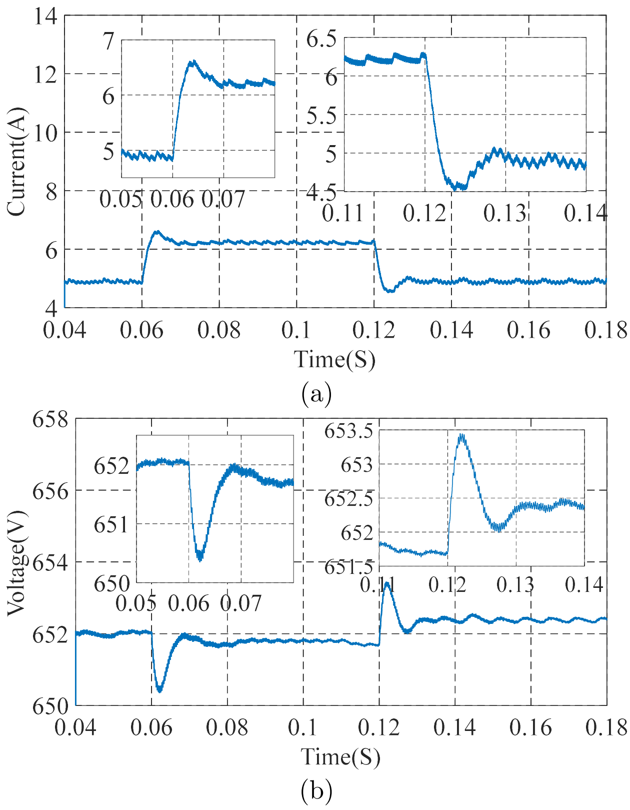

Fig. 5. Simulation result using dual closed-loop PI when the battery voltage is step changed between 22V and 28V. (a) Inductor current. (b) Output voltage.

Fig. 5 shows the simulation results applied dual closed-loop PI, with the inner loop $K_{p1} = 0.5$, $K_{i1} = 0.012$ and outer loop $K_{p2} = 0.04$, $K_{i2} = 0.001$. Due to the parasitic resistors in L and C, the output voltage cannot be stable without a steady-state error. During these three modes, the stable output voltage are $652V$, $651.8V$ and $652.5V$, and the steady-state error are $2.0V$, $1.8V$ and $2.5V$. It indicates that steady-state error exists in all these modes, which increases with the variable load. From mode 1 to mode 2, the transient time is $15ms$. The peak ripple voltage and current are $650.5V$ and $6.6A$, respectively. From mode 2 to mode 3, the transient time is $15ms$. The peak ripple voltage and current are $653.5V$ and $4.5A$, respectively.

The simulation results using this proposed controller are shown in Fig. 6. The parameters of compensation PI are $K_p = 1.2$, $K_i = 0.055$ and the virtual impedance $r_1 = 25$. Due to the complementary effect, the stable output voltage in these three modes are $650V$ without steady-state error. From mode 1 to mode 2, the transient time is $5ms$. The peak ripple voltage and current are $649.3V$ and $7.3A$, respectively. From mode 2 to mode 3, the transient time is $5ms$. The peak ripple voltage and current are $651.1V$ and $5A$, respectively.

Simulation results show that the proposed controller has a much better response performance, and the transient time is three times less than that using dual closed-loop

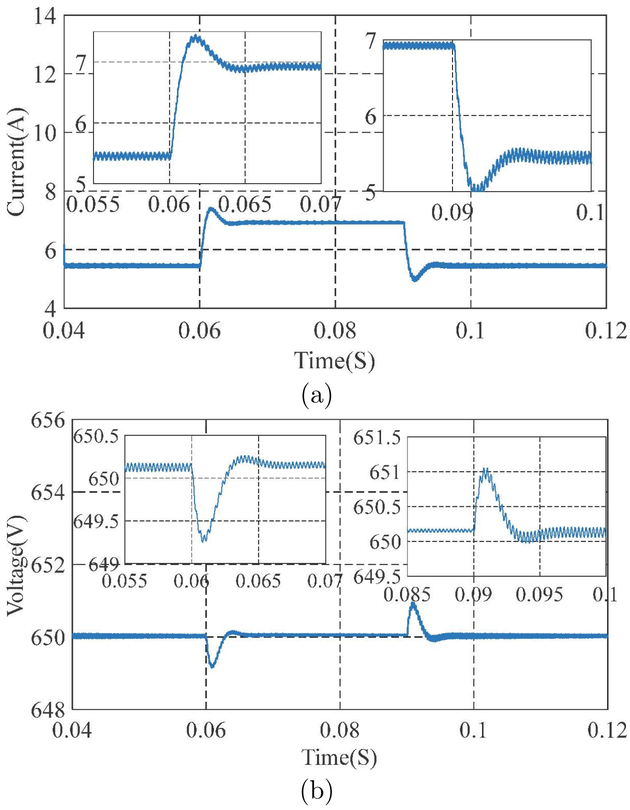

Fig. 6. Simulation result using PI-PBC when the battery voltage is step changed between 22V and 28V. (a) Inductor current. (b) Output voltage.

PI controller. The output voltage of DC/DC converter is regulated to desired value without steady-state error. In addition, comparing Fig. 5 with Fig. 6, it indicates that the ripple wave in voltage is much smaller than that using dual closed-loop PI controller. A relatively more stable duty ratio is achieved, which meets the working requirement of IGBT.

5. CONCLUSION

This paper has proposed a PBC and compensation designing method for AGVs WPT system. The proposed control has achieved desired systematic charging power by regulating the output voltage of DC/DC converter. With the principle of the impedance matching method, the LCC-LCC resonant network has been analyzed, then a stable resonance irrelevant with the mutual inductor and output load has been obtained. A PI controller has been designed to operate with PBC to eliminate the steady-state error. Simulation results have shown that the proposed control scheme and designing method not only can ensure the stability but also achieves desired response performance of the system.

REFERENCES

Lu, F., Zhang, H., Zhu, C., Diao, L., Gong, M., Zhang, W., & Mi, C. C. (2019). A Tightly Coupled Inductive Power Transfer System for Low-Voltage and High-Current Charging of Automatic Guided Vehicles. *IEEE Transactions on Power Electronics*, 66(9), 6867–6875.

RamRakhyani A. K., Mirabbasi S., Chiao M. (2010). Design and optimization of resonance-based efficient wireless power delivery systems for biomedical implants. *IEEE Transactions on Biomedical Circuits and Systems*, 5(1):48–63.

Zhang, Z., Pang, H., Georgiadis, A., & Cecati, C. (2018). Wireless power transfer – An overview. *IEEE Transactions on Industrial Electronics*, 66(2), 1044–1058.

Feng, H., Cai, T., Duan, S., Zhao, J., Zhang, X., & Chen, C. (2016). An LCC-compensated resonant converter optimized for robust reaction to large coupling variation in dynamic wireless power transfer. *IEEE Transactions on Industrial Electronics*, 63(10), 6591–6601.

Li, S., Li, W., Deng, J., Nguyen, T. D., & Mi, C. C. (2014). A double-sided LCC compensation network and its tuning method for wireless power transfer. IEEE Transactions on Vehicular Technology. *IEEE Transactions on Vehicular Technology*, 64(6), 2261–2273.

Xiao, C., Cheng, D., & Wei, K. (2018). An LCC-C compensated wireless charging system for implantable cardiac pacemakers: Theory, experiment, and safety evaluation. *IEEE Transactions on Power Electronics*, 33(6), 4894–4905.

Jeltsema, D., Scherpen, J. M. (2004). Tuning of passivity – preserving controllers for switched-mode power converters. *IEEE Transactions on Automatic Control*, 49(8), 1333–1344.

Ortega, R., Garcia–Canseco, E. (2004). Interconnection and damping assignment passivity-based control: A survey. *European Journal of control*, 10(5), 432–450.

Son, Y. I., Kim, I. H. (2011). Complementary PID controller to passivity-based nonlinear control of boost converters with inductor resistance. *IEEE Transactions on Control Systems Technology*, 20(3), 826–834.

Zeng, J. W., Zhang, Z. and Qiao, W. (2014). An interconnection and damping assignment passivity-based controller for a DC/DC boost converter with a constant power load. *IEEE Transactions on Industrial Electronics*, 50(4), 2314–2322.